Alexey Klechikov, Guillaume Mercier, Tiva Sharifi, Igor A. Baburin, Gotthard Seifert, Alexandr V. Talyzin

Hydrogen storage in high surface area graphene scaffolds

Erstveröffentlichung in / First published in:
Chemical Communications. 2015, 51(83), S. 15280--15283 [Zugriff am: 01.11.2019]. Royal Society of Chemistry. ISSN 1364-548X.

DOI: https://doi.org/10.1039/c5cc05474e

ChemComm

COMMUNICATION

View Article Online
View Journal | View Issue

Cite this: *Chem. Commun.*, 2015, 51, 15280

Received 3rd July 2015,
Accepted 19th August 2015

DOI: 10.1039/c5cc05474e

www.rsc.org/chemcomm

Hydrogen storage in high surface area graphene scaffolds†

Alexey Klechikov,[a] Guillaume Mercier,[a] Tiva Sharifi,[a] Igor A. Baburin,[b] Gotthard Seifert[b] and Alexandr V. Talyzin*[a]

Using an optimized KOH activation procedure we prepared highly porous graphene scaffold materials with SSA values up to 3400 $m^2 g^{-1}$ and a pore volume up to 2.2 $cm^3 g^{-1}$, which are among the highest for carbon materials. Hydrogen uptake of activated graphene samples was evaluated in a broad temperature interval (77–296 K). After additional activation by hydrogen annealing the maximal excess H_2 uptake of 7.5 wt% was obtained at 77 K. A hydrogen storage value as high as 4 wt% was observed already at 193 K (120 bar H_2), a temperature of solid CO_2, which can be easily maintained using common industrial refrigeration methods.

Carbon materials with ultra-high surface area are of increasing interest for several important energy-related applications: hydrogen storage,[1] supercapacitors,[2,3] and batteries.[4] Therefore, a lot of efforts have been made during the past decades on studies of hydrogen storage in various nanostructured porous materials: activated carbons,[5,6] carbon nanotubes, templated carbons,[7,8] carbide derived carbons[9] and, more recently, graphene.[10–13]

The theoretical SSA of ideal single layered graphene is about 2630 $m^2 g^{-1}$ which is often cited as the maximal possible value.[14] Recent theoretical modelling results demonstrated that SSA values as high as 5000 $m^2 g^{-1}$ are possible for graphene sheets perforated with small size holes and packed into a 3D structure with an optimal inter-layer distance of 0.7–1 nm.[15] However, there are no suitable methods to hold graphene layers separate from each other.

The best of the so far known methods to produce highly porous carbon materials is KOH activation, which was extensively studied for a broad range of precursors, including natural biomaterials and, more recently, reduced graphene oxide (r-GO).[2,3,11] It is known that the SSA of carbons produced by KOH activation can be as high as ~3000 $m^2 g^{-1}$ and depends very strongly on the type of the precursor materials.[4] Using graphene as a precursor can be an advantage due to the more precisely defined shape and possibility to arrange graphene sheets into multilayered structures. Introducing defects *e.g.* wrinkles, holes and wave-like corrugations could prevent graphene sheets from aggregating into less porous graphitic structures. Activation of r-GO using annealing with KOH was reported to result in samples with a SSA of 3100 $m^2 g^{-1}$ and with an extraordinarily high pore volume of 2.14 $cm^3 g^{-1}$,[2,11] which is superior to those of other carbon materials. Typical pore volumes below 1.4 $cm^3 g^{-1}$ have been reported for carbon materials produced using KOH activation of precursors other than graphene, even for samples with SSA values exceeding 3000 $m^2 g^{-1}$.[4] A lower total pore volume of ~1.7 $cm^3 g^{-1}$ was reported also for zeolite-templated carbons with a SSA of about 3300 $m^2 g^{-1}$.[16] Therefore, it is rather interesting to verify hydrogen sorption parameters of KOH activated r-GO samples (a-r-GO) with ultra-high surface area and pore volume.

Rapid thermal exfoliation of graphite oxides results in the formation of r-GO consisting of strongly defective single-layered and few-layered graphene sheets.[17] However the SSA of this r-GO is relatively small (up to ~800 $m^2 g^{-1}$). Much higher SSA of KOH-activated samples has been attributed to the formation of holes in graphene sheets as revealed *e.g.* by direct electron microscopy observations.[2,11,18] However, hydrogen storage parameters of KOH activated samples with an ultra-high SSA of ~3000 $m^2 g^{-1}$ were not reported in these studies.

Recently we re-evaluated hydrogen sorption properties of "graphene" with a broad range of SSA (300–2400 $m^2 g^{-1}$), including some samples prepared using the KOH activation procedure.[13] However, initially we were not able to reproduce SSA approaching 3000 $m^2 g^{-1}$ following a procedure described in ref. 11. Lower SSA values have also been reported in several later studies aimed at KOH activation of graphene-related materials.[19–21]

Here we report an optimized procedure for KOH activation of r-GO which allows us to produce reliable and reproducible materials with SSA up to 3400 $m^2 g^{-1}$ and a pore volume of 2.2 $cm^3 g^{-1}$ and to evaluate hydrogen storage parameters of activated r-GO (a-r-GO). Therefore, we extended the H_2 uptake *vs.* SSA trends (at 296 K and 77 K) to include a broader range of values (300–3300 $m^2 g^{-1}$).

[a] *Department of Physics, Umeå University, SE-901 87 Umeå, Sweden. E-mail: alexandr.talyzin@physics.umu.se*
[b] *Technische Universität Dresden, Theoretische Chemie, Bergstraße 66b, 01062 Dresden, Germany*

† Electronic supplementary information (ESI) available. See DOI: 10.1039/c5cc05474e

r-GO obtained by thermal exfoliation of Hummers graphite oxide was subjected to modified KOH activation tuned to provide samples with an ultra-high surface area of over 3000 $m^2 g^{-1}$ (see the ESI† for details). Hydrogen storage parameters were determined in a broad temperature interval using the volumetric method. Several samples were also annealed *in situ* in 50 bar H_2 gas at 673–723 K which resulted in a further increase of H_2 uptakes.

The SSA of activated r-GO (a-r-GO) samples was evaluated using nitrogen adsorption isotherms (Fig. 1a). This isotherm analysed using the BET method provides an SSA value of 3300 $m^2 g^{-1}$. The analysis of the isotherm shown in Fig. 1a by the quenched solid density functional theory (QSDFT) method based on a slit-pore model results in a lower value of 2620 $m^2 g^{-1}$, while the nonlocal density functional theory (NLDFT) method based on a slit/cylindrical-pore model shows 2660 $m^2 g^{-1}$. In the following discussions we use SSA values determined by the BET method. Two peaks are typically observed in the pore size distribution plots simulated for a-r-GO using slit pore QSDFT (Fig. 1c), the first peak centered approximately at 0.7–0.8 nm and the second at ~1.5 nm. The "graphene scaffold" structure created using the KOH activation procedure shows essentially microporous nature in contrast to pristine r-GO obtained by thermal exfoliation (Fig. 1c).

Several a-r-GO samples were additionally annealed in H_2 in order to substitute oxygen containing functional groups with hydrogen. These samples showed a pore size distribution with an additional peak corresponding to wider pores with up to ~3 nm (see the ESI†). Analysis of pore size distribution for samples with the highest SSA shows that a-r-GO is essentially microporous with the size of pores below 3 nm, a maximal BET surface area of 3300 $m^2 g^{-1}$ and a pore volume up to 2.22 $cm^3 g^{-1}$ (Fig. 1b). The pore volume of a-r-GO samples is superior compared to other nanoporous materials. For example, a comparable pore volume of ~2 $cm^3 g^{-1}$ is achieved in Metal Organic Framework (MOF) materials with about twice higher SSA values (~5000–7000 $m^2 g^{-1}$).[22,23] Note that changing the model from slit pores to slit-cylindrical pores results in a rather small change in the pore volume (Fig. S1 in the ESI†).

The evolution of the sample composition as a result of GO exfoliation and activation was evaluated using XPS (Fig. S2 in the ESI†). The composition of the precursor GO sample corresponds to C/O = 2.63 and increases up to C/O = 6.3 after thermal reduction. Annealing of an r-GO/KOH mixture resulted in further reduction (C/O = 24.0), whereas after hydrogen annealing a-r-GO showed C/O = 35.

Both r-GO and a-r-GO samples are non-crystalline solids and show no diffraction peaks. There is also no change in Raman spectra as a result of activation treatment (Fig. S3 in the ESI†). Therefore, the microstructure of a-r-GO samples was evaluated also by Scanning Electron Microscopy (SEM) which showed that they consist of grains with a size of up to tens of micrometers (Fig. 2).

The grains exhibit a hierarchical porous structure with typical shapes of observed grains from cheese-like to sponge-like depending on the number of micrometer sized holes (see also the ESI†). Under higher magnification, smaller pores with a typical size on the scale of

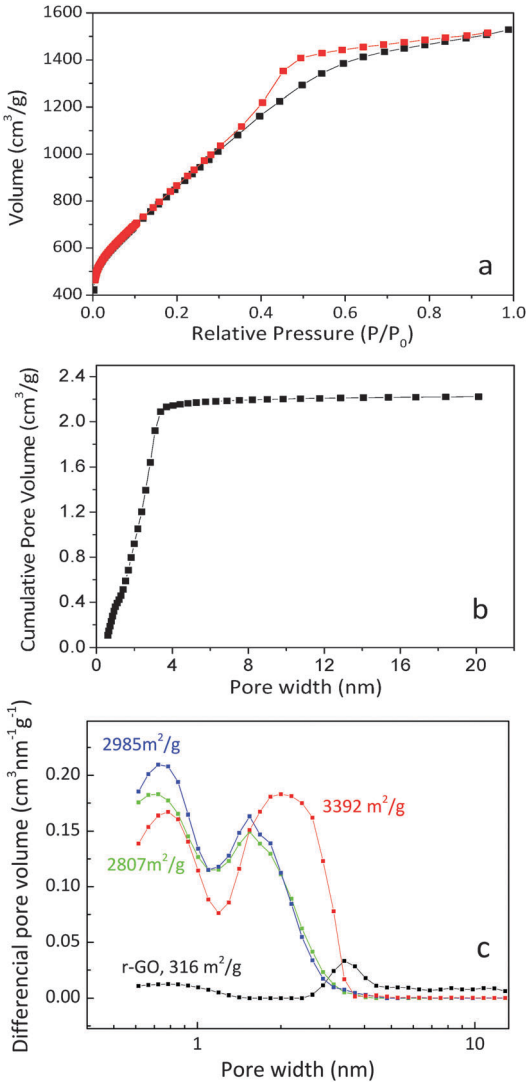

Fig. 1 N2 adsorption/desorption isotherm for the a-r-GO sample (SSA = 3300 $m^2 g^{-1}$) (a) and analysis of isotherms simulated using the QSDFT slit pore model: plot of cumulative pore volume (b), pore size distribution for several a-r-GO samples (c).

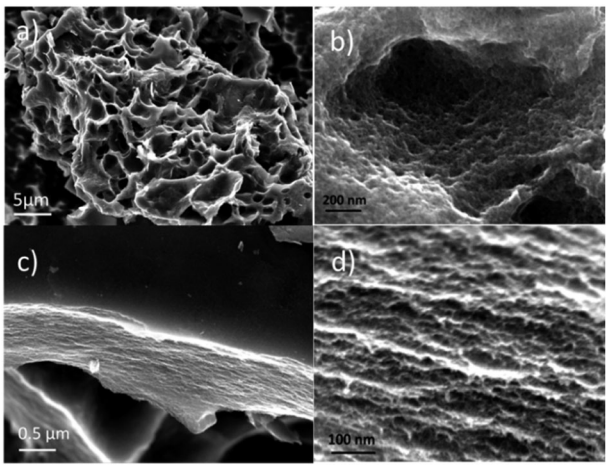

Fig. 2 SEM images recorded for the a-r-GO sample with a BET surface area of ~3300 $m^2 g^{-1}$. The images show a hierarchical size pore network (a and b) and also some layered structure on the broken grain edge (c and d).

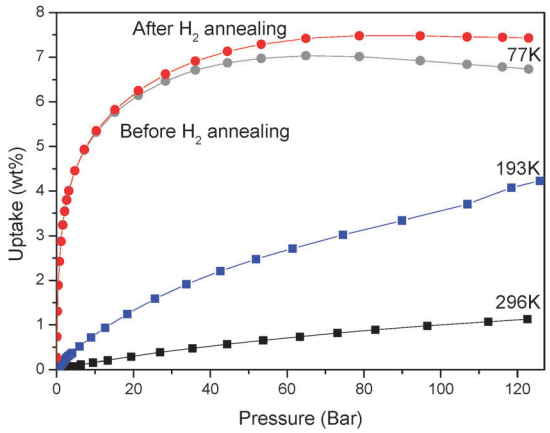

Fig. 3 Excess adsorption isotherms at T = 77 K, T = 193 K and T = 296 K for the a-r-GO sample with SSA = 3230 m^2 g^{-1} and isotherm recorded at 77 K after H2 annealing.

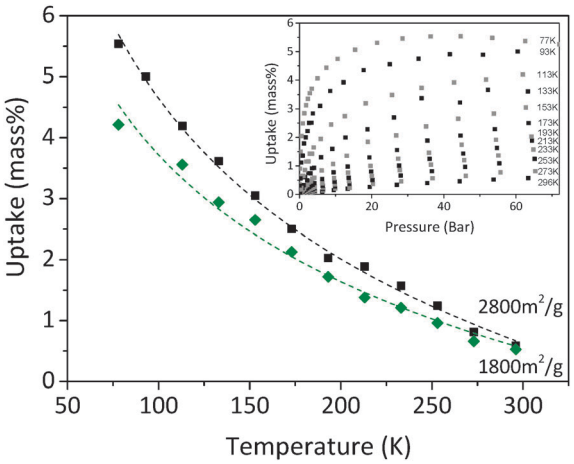

Fig. 4 Temperature dependence of H_2 uptakes for two a-r-GO samples. The inset shows isotherms recorded for the a-r-GO sample with a BET surface area of 2800 m^2 g^{-1} at different temperatures up to a pressure of 65 bar H_2. The isosteric heat of adsorption value of 6.1 kJ mol^{-1} was determined for this sample.

a few nanometers to tens of nanometers are revealed. A more detailed study showed that broken skeleton-like walls of a-r-GO grains exhibit clearly layered texture (Fig. 2c and d). Fig. 2c shows the edge view of a densely packed array of irregularly curved and interconnected layers. The overall structure of our samples can then be described as packs of strongly perforated graphene layers arranged into 3D "scaffolds".

Hydrogen sorption of a-r-GO samples was evaluated using the volumetric method at 77 K and 296 K. An example of H_2 isotherms recorded for a high surface area a-r-GO sample (SSA = 3230 m^2 g^{-1}) is shown in Fig. 3. The H_2 uptake measured at 77 K saturates at ~40 bar (7.04 wt%) whereas at 296 K adsorption is not saturated and reaches 1.13 wt% at 120 bar. The hydrogen uptake was further improved using additional activation by H_2 annealing at 450 °C for 2 hours. Remarkably, hydrogen uptakes measured for the annealed sample increased by ~10% (1.25 wt% at 296 K and 7.48 wt% at 77 K). Nitrogen isotherms were recorded for this sample before H_2 uptake measurements, after H_2 measurements, and finally after H_2 annealing and re-measurement of hydrogen sorption on an annealed sample (Sample 2 in Table S1, ESI†) showing only negligible variation. Therefore, the increase of hydrogen sorption as an effect of H_2 annealing should be assigned to a change in the pore size distribution, rather than to an increase of SSA (Fig. 1c and Fig. S2 in ESI†). High hydrogen sorption properties of material are preserved even after prolonged exposure to air and are reversible for several cycles (Fig. S4, ESI†)

The temperature dependence of hydrogen uptake measured for two a-r-GO samples is shown in Fig. 5. The plot includes saturation values for lower temperatures and uptake values specific for 65 bar H_2 pressure for higher temperatures when saturation could not be achieved (inset in Fig. 4). Hydrogen uptakes for samples with maximal surface area were also verified at a higher H_2 pressure of 120 bar for temperature points of practical interest: 273 K (ice bath) and 193 K (temperature of solid CO_2) (Table 1 in the ESI†). Remarkably, hydrogen storage with a capacity as high as 3.8–4.2 wt% can be achieved already at a solid CO_2 temperature. Note that this value measured at 120 bar H_2 is not saturated and can be further improved by an increase in pressure. Very common industrial refrigeration methods allow maintaining samples at 193 K which can be of practical interest for hydrogen storage.

The isosteric heat of adsorption for the sample with maximal storage capacity (Fig. 3) was evaluated using four isotherms (following the procedure described in ref. 24). The Q_{st} value of ~6.2–6.4 kJ mol^{-1} can be obtained by rough extrapolation of the adsorption heat to zero uptake (Fig. S5 in the ESI†). This value is in good agreement with the data reported earlier for high surface area carbon materials (*e.g.* 6.5 kJ mol^{-1} for the sample with a SSA of 3591m^2 g^{-1} (ref. 7) and 5.9 kJ mol^{-1} for r-GO[10]).

The results of hydrogen sorption measurements are summarized in Fig. 5 which shows SSA *vs.* wt% trends at 77 K and 296 K. It is known that hydrogen uptakes by various carbon materials correlate with BET SSA and show common trends.[8,25–27] Some early studies of hydrogen adsorption by "graphene" reported H_2 uptake values

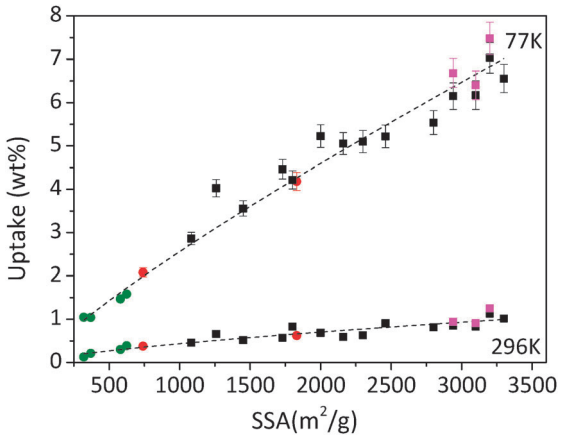

Fig. 5 H_2 uptake (wt%) *vs.* SSA trends evaluated using the volumetric method and immersion cell for a-r-GO samples at 296 K (120 bar) and 77 K (saturation value) before (■) and after H_2 annealing (■). The trend is extended showing samples of r-GO (●)[13] and reference points for mesoporous carbon and activated carbon (●).

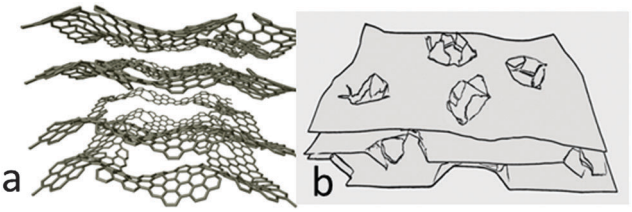

Fig. 6 Schematic representation of a possible a-r-GO structure consisting of strongly defective fragments of graphene flakes (a) and a more general scheme showing how the ruptured hole edges can serve as "pillars" for graphene scaffolds (b).

3–10 fold higher for r-GO samples with relatively small SSA values.[28,29] However, our experiments demonstrate that H_2 uptakes of "graphene" samples follow standard for all carbon material trends. The trends revealed in Fig. 5 demonstrate 0.32 and 2.3 wt% H_2 uptakes per 1000 $m^2\ g^{-1}$ for 296 K and 77 K, respectively, in good agreement with the "Chahine rule".[7,30]

An interesting example of deviation from the standard trends is activation of a-r-GO by H_2 annealing. The increase of H_2 uptakes occurs after hydrogen annealing activation without visible change in surface area values or the total pore volume, only with some change in pore size distribution (Fig. S2 in ESI†). Most likely the effect of H_2 annealing at 723 K is substitution of residual oxygen containing functional groups on the edges of a-r-GO pores with smaller hydrogen atoms. We suggest that the increase of H_2 uptakes could be explained by contribution of sub-nanometer pores which become accessible for hydrogen as a result of pore broadening by hydrogenation.

The structure of KOH activated material was cited in some previous publications simply as "activated graphene". However, it is obvious from images shown in Fig. 2 that the samples need to be considered as three-dimensionally arranged irregular packing of strongly defective graphene layers (Fig. 6a). The powder of r-GO typically has very low bulk density with individual few layered graphene flakes not bound to each other. Annealing with KOH results in the formation of solid micrometer size grains which consist of more densely packed and interconnected perforated graphene sheets. The role of pillaring units separating graphene sheets from each other could be played *e.g.* by ruptured edges of holes (Fig. 6b). The irregular shape of r-GO flakes and defects created by gasification prevents formation of a graphitic structure.

The maximal SSA observed in our experiments was $\sim$3400 $m^2\ g^{-1}$. The SSA values over 3000 $m^2\ g^{-1}$ were reproduced in at least 15 separately annealed samples. These values are comparable to the highest reported for nanostructured carbons, but still below 4000–5000 $m^2\ g^{-1}$ theoretically predicted for highly porous perforated ordered graphene multilayers which promises even further improved hydrogen storage of graphene scaffolds.[16]

In conclusion, KOH activation of thermally exfoliated r-GO was tuned to produce samples with an ultra-high BET surface area up to $\sim$3400 $m^2\ g^{-1}$ and a pore volume up to 2.2 $cm^3\ g^{-1}$, superior to any other carbon materials. Furthermore, our graphene-based materials successfully compete with MOFs regarding the pore volume and hydrogen storage properties.[22,23] As a result of activation treatment r-GO is transformed into a three-dimensional structure composed of strongly defective and interconnected graphene layers. Hydrogen storage parameters of graphene scaffolds produced by KOH activation measured for the a-r-GO sample with a SSA of $\sim$3230 $m^2\ g^{-1}$ after additional activation using high temperature annealing in hydrogen gas were 1.25 wt% at 293 K (120 bar), 1.61 wt% at 273 K (120 bar), 4.23 wt% (120 bar) at 193 K (temperature of solid CO_2) and $\sim$7.48 wt% (saturation value) at 77 K.

This work was financially supported by the Swedish Research Council, Grant no. 621-2012-3654 (A.T.) and by the Graphene Flagship (contract no. NECT-ICT-604391). We thank A. Shchukarev for help with XPS analysis.

Notes and references

1 K. Spyrou, D. Gournis and P. Rudolf, *ECS J. Solid State Sci. Technol.*, 2013, **2**, M3160–M3169.
2 L. L. Zhang, X. Zhao, M. D. Stoller, Y. W. Zhu, H. X. Ji, S. Murali, Y. P. Wu, S. Perales, B. Clevenger and R. S. Ruoff, *Nano Lett.*, 2012, **12**, 1806–1812.
3 L. Zhang, F. Zhang, X. Yang, G. K. Long, Y. P. Wu, T. F. Zhang, K. Leng, Y. Huang, Y. F. Ma, A. Yu and Y. S. Chen, *Sci. Rep.*, 2013, **3**, 1408.
4 J. C. Wang and S. Kaskel, *J. Mater. Chem.*, 2012, **22**, 23710–23725.
5 M. A. de la Casa-Lillo, F. Lamari-Darkrim, D. Cazorla-Amoros and A. Linares-Solano, *J. Phys. Chem. B*, 2002, **106**, 10930–10934.
6 M. Jorda-Beneyto, F. Suarez-Garcia, D. Lozano-Castello, D. Cazorla-Amoros and A. Linares-Solano, *Carbon*, 2007, **45**, 293–303.
7 N. P. Stadie, J. J. Vajo, R. W. Cumberland, A. A. Wilson, C. C. Ahn and B. Fultz, *Langmuir*, 2012, **28**, 10057–10063.
8 H. L. Wang, Q. M. Gao and J. Hu, *J. Am. Chem. Soc.*, 2009, **131**, 7016–7022.
9 G. Yushin, R. Dash, J. Jagiello, J. E. Fischer and Y. Gogotsi, *Adv. Funct. Mater.*, 2006, **16**, 2288–2293.
10 G. Srinivas, Y. W. Zhu, R. Piner, N. Skipper, M. Ellerby and R. Ruoff, *Carbon*, 2010, **48**, 630–635.
11 Y. W. Zhu, S. Murali, M. D. Stoller, K. J. Ganesh, W. W. Cai, P. J. Ferreira, A. Pirkle, R. M. Wallace, K. A. Cychosz, M. Thommes, D. Su, E. A. Stach and R. S. Ruoff, *Science*, 2011, **332**, 1537–1541.
12 V. Tozzini and V. Pellegrini, *Phys. Chem. Chem. Phys.*, 2013, **15**, 80–89.
13 A. G. Klechikov, G. Mercier, P. Merino, S. Blanco, C. Merino and A. V. Talyzin, *Microporous Mesoporous Mater.*, 2015, **210**, 46–51.
14 K. R. Matranga, A. L. Myers and E. D. Glandt, *Chem. Eng. Sci.*, 1992, **47**, 1569–1579.
15 I. A. Baburin, A. Klechikov, G. Mercier, A. V. Talyzin and G. Seifert, *Int. J. Hydrogen Energy*, 2015, **40**, 6594–6599.
16 H. Nishihara, P. X. Hou, L. X. Li, M. Ito, M. Uchiyama, T. Kaburagi, A. Ikura, J. Katamura, T. Kawarada, K. Mizuuchi and T. Kyotani, *J. Phys. Chem. C*, 2009, **113**, 3189–3196.
17 A. V. Talyzin, T. Szabo, I. Dekany, F. Langenhorst, P. S. Sokolov and V. L. Solozhenko, *J. Phys. Chem. C*, 2009, **113**, 11279–11284.
18 Z. Li, B. Song, Z. K. Wu, Z. Y. Lin, Y. G. Yao, K. S. Moon and C. P. Wong, *Nano Energy*, 2015, **11**, 711–718.
19 S. W. Wang, F. Tristan, D. Minami, T. Fujimori, R. Cruz-Silva, M. Terrones, K. Takeuchi, K. Teshima, F. Rodriguez-Reinoso, M. Endo and K. Kaneko, *Carbon*, 2014, **76**, 220–231.
20 B. Zheng, T. W. Chen, F. N. Xiao, W. J. Bao and X. H. Xia, *J. Solid State Electrochem.*, 2013, **17**, 1809–1814.
21 G. Srinivas, J. Burress and T. Yildirim, *Energy Environ. Sci.*, 2012, **5**, 6453–6459.
22 I. Senkovska and S. Kaskel, *Chem. Commun.*, 2014, **50**, 7089–7098.
23 N. Klein, I. Senkovska, I. A. Baburin, R. Grunker, U. Stoeck, M. Schlichtenmayer, B. Streppel, U. Mueller, S. Leoni, M. Hirscher and S. Kaskel, *Chem. – Eur. J.*, 2011, **17**, 13007–13016.
24 B. Schmitz, U. Muller, N. Trukhan, M. Schubert, G. Ferey and M. Hirscher, *ChemPhysChem*, 2008, **9**, 2181–2184.
25 B. Assfour, S. Leoni, G. Seifert and I. A. Baburin, *Adv. Mater.*, 2011, **23**, 1237–1241.
26 M. Hirscher and M. Becher, *J. Nanosci. Nanotechnol.*, 2003, **3**, 3–17.
27 B. Panella, M. Hirscher and S. Roth, *Carbon*, 2005, **43**, 2209–2214.
28 A. Ghosh, K. S. Subrahmanyam, K. S. Krishna, S. Datta, A. Govindaraj, S. K. Pati and C. N. R. Rao, *J. Phys. Chem. C*, 2008, **112**, 15704–15707.
29 C. C. Huang, N. W. Pu, C. A. Wang, J. C. Huang, Y. Sung and M. D. Ger, *Sep. Purif. Technol.*, 2011, **82**, 210–215.
30 E. Poirier, R. Chahine and T. K. Bose, *Int. J. Hydrogen Energy*, 2001, **26**, 831–835.